Durability enhancement of novel monolithic metal supported Solid Oxide Fuel Cells through processing optimizations

Pirou, Stéven; Talic, Belma; Brodersen, Karen; Skafte, Theis Løye; Hauch, Anne; Høgh, Jens Valdemar Thorvald; Henriksen, Henrik; Persson, Åsa Helen; Hagen, Anke

Published in:
International Journal of Hydrogen Energy

Link to article, DOI:
10.1016/j.ijhydene.2022.12.139

Publication date:
2023

Document Version
Publisher's PDF, also known as Version of record

Available online at www.sciencedirect.com

ScienceDirect

journal homepage: www.elsevier.com/locate/he

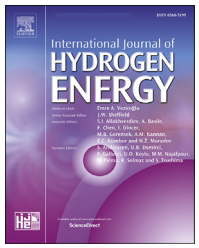

Durability enhancement of novel monolithic metal supported Solid oxide fuel cells through processing optimizations

Stéven Pirou[*], *Belma Talic*[1], *Karen Brodersen*[2], *Theis Løye Skafte*[3], *Anne Hauch, Jens Valdemar Thorvald Høgh, Henrik Henriksen, Åsa Helen Persson, Anke Hagen*

Department of Energy Conversion and Storage, Technical University of Denmark, Anker Engelunds Vej, Buildings 301 and 310, 2800, Kgs. Lyngby, Denmark

HIGHLIGHTS

- A novel monolithic metal-supported SOFC is designed, manufactured and tested.
- Advanced co-casting and co-sintering methods are used to produce the cells.
- Seal composition and layer assembly method are crucial criteria for cell durability.
- Processing optimizations improved the cell durability by a factor of 100.
- Preliminarily electrochemical tests displayed a resistance of ~0.7 Ωcm^2 at 750 °C.

ARTICLE INFO

Article history:
Received 24 August 2022
Received in revised form
27 November 2022
Accepted 11 December 2022
Available online 2 January 2023

Keywords:
Solid oxide fuel cell
Monolith
Metal supported
Cell design
Electrochemical performance & durability
Processing optimizations

ABSTRACT

In the last decades, Solid Oxide Fuel Cells (SOFCs) have received a lot of attention due to their ability to efficiently convert hydrogen and other fuels to electricity and heat. Cells with different designs (planar, tubular, anode-, electrolyte-, metal-supported) have been intensively studied in terms of performance, costs and lifetime. Still, technical challenges such as limited thermal cycling stability and cost-efficient paths to up-scaling need to be solved to make the SOFC technology more commercially attractive. This study presents the design, fabrication and testing of a novel monolithic metal-supported SOFC with the aim to achieve thermal cycling robustness and a high volumetric power density using cost-competitive and scalable manufacturing methods. The study presents preliminary electrochemical performances of the cells and key parameters of the manufacturing process that were optimized to increase the stability/durability of the monolith by a factor of 100.

* *Corresponding author.*
E-mail addresses: spir@topsoe.com (S. Pirou), Belma.Talic@sintef.no (B. Talic), k.brodersen4070@gmail.com (K. Brodersen), theis@noon.energy (T.L. Skafte), ahau@topsoe.com (A. Hauch), jvth@topsoe.com (J.V.T. Høgh), hhen@dtu.dk (H. Henriksen), aase@dtu.dk (Å.-H. Persson), anke@dtu.dk (A. Hagen).
[1] Belma Talic: SINTEF, Forskningsveien 1, 0373 Oslo, Norway.
[2] Stéven Pirou, Karen Brodersen, Anne Hauch and Jens Valdemar Thorvald: Topsoe A/S, Haldor Topsøes Allé 1, 2800 Kgs. Lyngby, Denmark.
[3] Theis Løye Skafte: Noon Energy Inc., Palo Alto, 94306 California, USA.
https://doi.org/10.1016/j.ijhydene.2022.12.139

Introduction

In the last decades, Solid Oxide Fuel Cells (SOFCs) have attracted considerable interest because they offer a clean and efficient means of producing electricity from a variety of fuels. With this technology, hydrogen-containing or hydrogen-forming gas mixtures are electrochemically oxidized to convert chemical energy to electrical energy with high efficiencies (i.e. > 60%) and heat [1,2]. A single SOFC comprises a dense electrolyte layer made of an ionically conducting ceramic material sandwiched between two porous electrodes. Typical SOFC configurations include planar, tubular and flat-tubular designs [3–7], of which the planar and tubular configurations are the most used. The planar geometry presents the advantage of generally having lower ohmic losses than the tubular, leading to a superior stack performance and a higher volumetric power density. However, the up-scaling of planar SOFCs is a challenge due to the need for sufficiently gas-tight seals and costly due to the large number of manufacturing steps involved. Furthermore, the highly dynamic operation is limited by the poor thermal cycling stability of ceramic SOFCs [2,8,9].

A recent publication reported the design of a novel monolithic SOFC with integrated seals and gas flow channels that retains the advantages of the planar design, overcomes the challenges of gas-tightness and thermal robustness and delivers superior power density compared to conventional SOFC stack designs [10]. In the present study, the manufacturing procedure of the metal-based, monolithic cells fabricated by tape-casting, lamination and single-step co-firing is further described and key parameters of the manufacturing process improving greatly the durability of the cells are revealed. By using these low-cost processing methods and a single firing step, both production costs and time are significantly reduced compared to the fabrication of conventional, planar SOFCs.

In this context, monolithic refers to the sintering of the stack in one step and the absence of dedicated supporting layers as in conventional SOFCs. Two main types of monolithic SOFCs have been reported previously: (i) a metal-based monolith [10–12] and (ii) an all-ceramic monolith [13]. The design that we present here is metal-based, which offers some clear advantages in comparison to all-ceramic SOFC stacks, both conventional and monolithic. With a metal-supported monolith design, the mechanical robustness and the ability to withstand dynamic operation with fast start-up and thermal cycling is improved, while the gravimetric and volumetric power density can potentially be higher [14]. Consequently, metallic monolith SOFCs are well suited for applications requiring fast start-up or intermittent operation and high power density, e.g. as vehicle range extenders or other mobile applications.

Design of the monolithic SOFC

The configuration of the monolith unit cell and the stack is shown schematically in Fig. 1 and has been described in a recent publication [10]. The cell consists of a ~10 μm thick scandia-doped yttria-stabilized zirconia (ScYSZ) electrolyte, two ~15 μm thick ScYSZ-Fe22Cr seal/electrode/seal-layers, and two ~400 μm thick Fe22Cr gas distribution and interconnect layers combined in one layer. ScYSZ was chosen as the electrolyte material because of the good ionic conductivity at the desired operating temperature (40 mS cm^{-1} at 700 °C [15]), while ferritic stainless steel with 22% Cr (Fe22Cr) was selected for the metal layers to ensure a matching thermal expansion coefficient (TEC) and good corrosion resistance. The monolith structure has gas flow channels integrated between the electrode and the interconnect to efficiently feed gases directly to the electrodes. In this design, the gas channels on the air and fuel sides are perpendicular, giving a cross-flow configuration. This configuration gives larger thermal gradients compared to a co-flow configuration, however, it makes the gas supply easier for a monolithic architecture. After screening various gas channel geometries, a sufficiently small pressure-drop could be achieved with honeycomb-like channels with a void size of 250 × 500 μm^2. The lowest pressure drop estimated from SOFC relevant operation at 650 °C is 40 mbar(g) and 240 mbar(g) for the fuel- and air-side, respectively. The estimation is based on

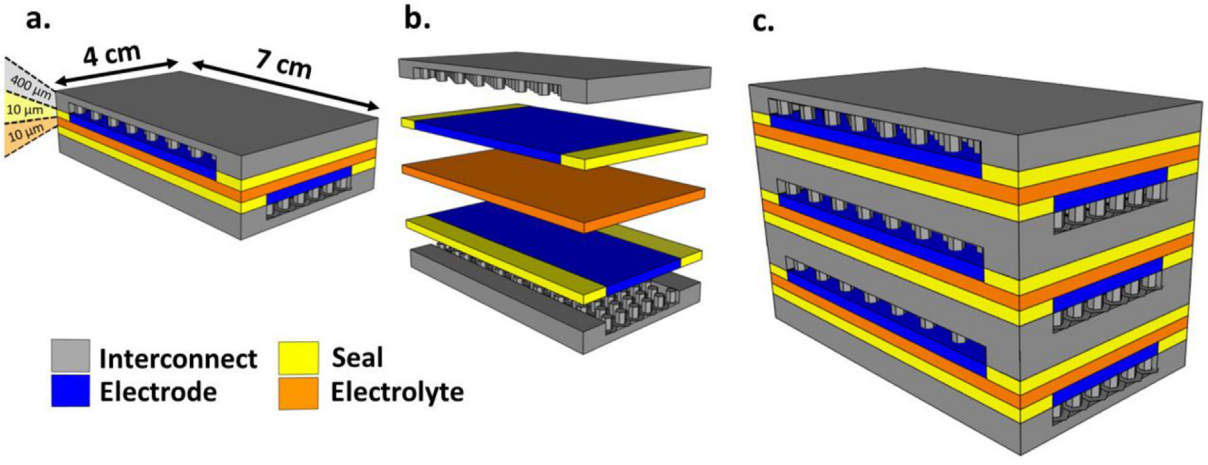

Fig. 1 – Design of the monolithic SOFCs. a. one-cell compact view, b. one-cell expanded view, showing the individual layers, and c. a three-cell stack compact view. Note that for clarity, the scale of the layers thickness is not respected.

fuel and air flow of 0.2 $_{N}$L/(h*cm^2) and 2 $_{N}$L/(h*cm^2), respectively, and an electrochemical active area of 18 cm^2.

Seals are integrated into the architecture of the monolith to ensure gas-tightness of the device, and to prevent gaseous and electronic crossover from one electrode to the other. The first objective of this design is to provide a SOFC in which the flow of fuel and oxidant gases is well controlled and in which no gas leakage detrimental to performance occurs. Thermal cycling stability, which is defined as the resistance to damage resulting from temperature changes and thermal gradients, is one of the most important requirements for mobile applications and is typically a major challenge for ceramic, planar SOFCs [16]. The poor thermal cycling stability of the conventional SOFCs is a result of small mismatches in the TEC of the different layers combined with the brittle nature of the ceramic cell and the glass-ceramic sealant [17]. The monolithic SOFC developed in this work is metal-based and has seals with a well-matched TEC integrated into the structure, thus improving the gas-tightness and the thermal cycling stability of the SOFC stack. The seals are placed in between the metallic interconnect layer and the ceramic electrolyte and are laterally joined to the cermet electrodes (see Fig. 1). A well-matching TEC to the adjacent layers is achieved by making the seal a composite of Fe22Cr (TEC_{Fe22Cr} = 10.9–11.2 10^{-6} K^{-1} in the temperature range 400–700 °C [18]) and ScYSZ (TEC_{ScYSZ} = 10.1–10.6 10^{-6} K^{-1} in the temperature range 400–700 °C [19]). Electronic crossover from one electrode to the other is prevented by limiting the content of the metal phase in seals to 20 vol%.

The design and fabrication methods of the monolithic SOFC presented in this work open up for the possibility to make a multi-cell stack in one single step, as shown in Fig. 1c. The component layers of the monolith can simply be stacked on top of each other, laminated together and co-sintered.

Thus, the metal-based monolithic SOFC stack design has the potential for the following characteristics.

- High power density per weight and volume
- Improved thermal cycling stability due to the choice of sealing materials and integration into the monolith
- Little or no need for stacking, lessening the risk of misalignment
- Low manufacturing cost for mass production due to minimal use of material and few processing steps
- Small thermal gradients due to the high thermal conductivity of metal, which allows for fast heating/cooling and dynamic operation

Experimental procedure

Single-cell monolith fabrication

The layers of the monolithic SOFC are produced by tape-casting, which is a well-established and relatively simple technique with a low implementation cost that can produce planar ceramic/metal sheets with a large area, good surface quality and controlled microstructure [20]. To overcome the challenges of gas-tightness and thermal robustness, a side-by-side tape-casting method is used to achieve good mechanical adhesion between the seals and the electrode layers. The side-by-side tape-casting is carried out using multiple slurries from individual doctor blade reservoirs.

Suspensions for side-by-side tape-casting of the seals and the electrode layer are manufactured by ball milling powders with a dispersant (polyvinyl pyrrolidone, PVP), a binder/plasticizers system (polyvinyl butyral, PVB, polyethylene glycol, triethylene glycol di-2-ethylhexanoate) and a solvent. After control of particle size and viscosity, the suspensions are de-aired and tape-casted using a doctor blade. The sealing layer suspension comprises ScYSZ and Fe22Cr powder in a 5:1 vol ratio. The electrode suspension comprises ScYSZ and Fe22Cr powder in a 1.67:1 vol ratio and contained graphite and poly(methyl methacrylate) (PMMA) powders as pore-formers. Scanning electron microscope (SEM) cross sectional analyses attested that the sintered porosity of the electrode is about 50%, with an average pore size of about 4 μm. For tape-casting, the suspensions are poured to a doctor blade divided in compartments to obtain the desired seal/electrode/seal-structure, as shown Fig. 2a.

A so-called "pore-former" layer is obtained by tape casting a suspension of graphite and PMMA powder in a 1:1 vol ratio to a green thickness of about 500 μm. The green pore-former tape is laser-cut into a honeycomb shape to form gas flow channels with the desired geometry. As the pore-former tape contains only organics it entirely burns off during the debindering step, thereby creating gas channels of about 250 μm height and 500 μm width. The pore-former composition was optimized to minimize overpressure inside the microstructure during burn-out of the organics, as detailed in Ref. [10].

The pore-former honeycomb tape is laminated onto the electrode using heated rolls in a double roll set-up in one pass. An interconnect layer consisting of Fe22Cr powder in suspension is co-cast on top of this laminated structure. The result is shown in Fig. 2b. Two of such sheets are produced to be used as the fuel and oxygen electrode of the cell.

An electrolyte tape made of ScYSZ is prepared by tape-casting. The complete cell is formed by laminating this electrolyte tape between the two sheets containing the seals, electrode, gas channels, and interconnect using an isostatic press set at 85 °C and 30 MPa. The green monoliths are debindered at 600 °C for 4 h in air, and then sintered at 1290 °C for 6 h in reducing atmosphere. Fig. 2c and 2d presents top and side view pictures of sintered monoliths, respectively. Fig. 3 summarizes the manufacturing procedure of the single-cell monolith.

Catalyst precursors and cell infiltration

After sintering, electrocatalysts are infiltrated into the electrodes of the monolith. Stoichiometric amounts of Ce-, Gd- and Ni-nitrate salts ($Ce(NO_3)_3{\cdot}6H_2O$, $Gd(NO_3)_3{\cdot}xH_2O$ and $(NO_3)_3{\cdot}6H_2O$, respectively) are mixed with deionized (DI) water and a dispersant (Pluronic P123) to form the desired precursor, $Ni{-}Ce_{0.8}Gd_{0.2}O_{3-\delta}$ (Ni-CGO), for the fuel electrode electrocatalyst. For the oxygen side, Ce- and Gd-nitrate salts are mixed with DI water and P123 to make $Ce_{0.8}Gd_{0.2}O_{3-\delta}$ (CGO); and La-, Sr- and Co-nitrate salts ($La(NO_3)_3{\cdot}6H_2O$, $Sr(NO_3)_2{\cdot}6H_2O$, and $Co(NO_3)_2{\cdot}6H_2O$, respectively) are mixed with DI water and P123 to make $La_{0.6}Sr_{0.4}CoO_{3-\delta}$ (LSC). The

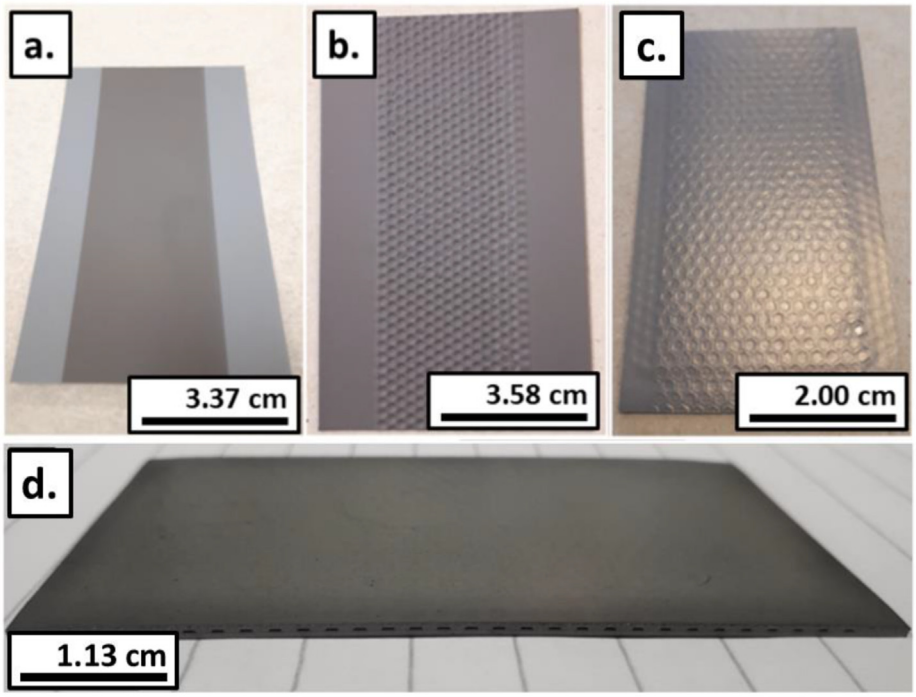

Fig. 2 – Pictures of monoliths throughout the fabrication process. a. seal/electrode/seal tape, b. interconnect layer co-cast on top of the honeycomb pore-former layer and side-by-side seal/electrode/seal, c. and d. top and side views of a sintered single-cell monolith, respectively.

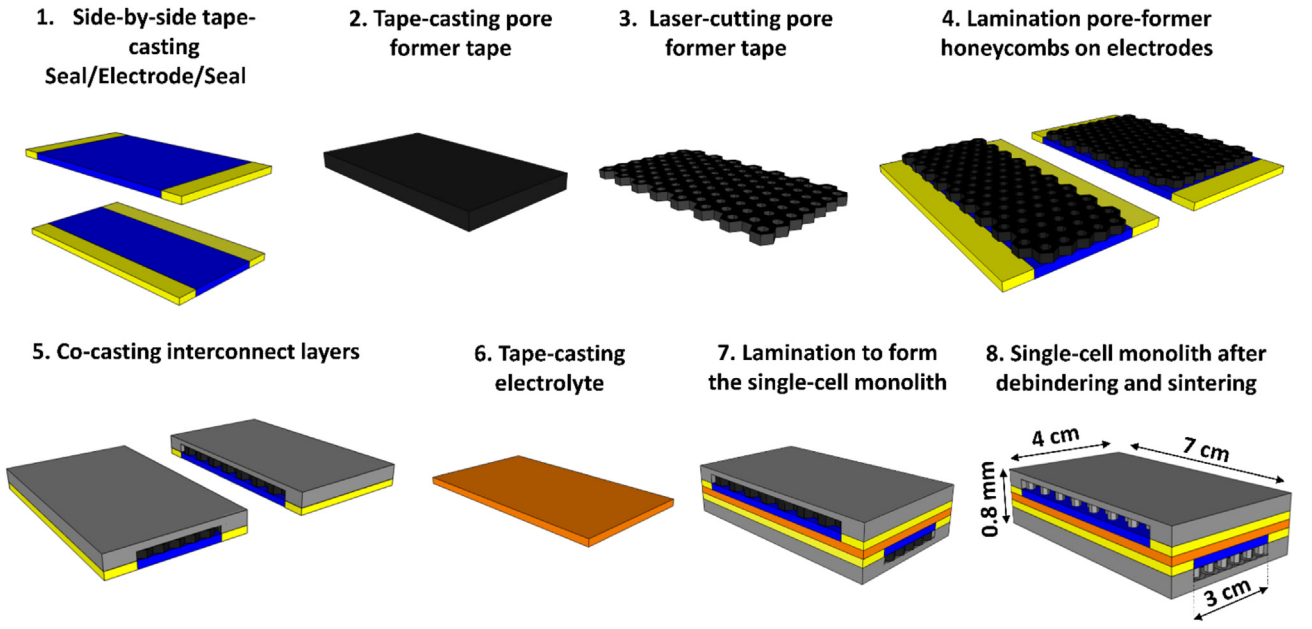

Fig. 3 – Manufacturing steps of single-cell monoliths.

concentration of the Ni-CGO, CGO and LSC solutions correspond to 1 M, 2 M and 1 M, respectively.

The infiltration process is carried out using a home-built infiltration tool, presented in Supplementary Fig. 1. Stainless steel clamps are screwed together with the monolith cells placed in an appropriately sized slit. Rubber rings are used to ensure that the cells stayed in place and that the precursor solution did not leak. The precursor solution is delivered via a dropper pipette. A small pressure is subsequently applied using an air gun to force the infiltration liquid through the electrode.

The monoliths are first infiltrated twice with CGO on both the electrode sides to form a thin ceramic barrier layer on the steel and thereby lessen corrosion during operation [21]. After each infiltration cycle of CGO, the cells are heated to 325 °C with a rate of 2 °C/min in stagnant air and held for 0.25 h

before cooling. This allows the evaporation of the water, decompose the nitrate salts and form the desired fluorite phase [22,23]. Following the first infiltration cycle of CGO, the monolith cells are additionally pre-oxidized by heating to 850 °C with a rate of 2 °C/min and holding for 2 h in 5% H_2/N_2. This is done as an additional effort to mitigate corrosion of the Fe22Cr steel [24] by forming an oxide-layer and has the added advantage of partially densifying the infiltrated CGO layer as well. Finally, the fuel and oxygen electrode are infiltrated with one cycle of Ni-CGO and LSC, respectively, and heat treated in air at 400 °C for 0.5 h.

Characterization techniques

Optical dilatometry is used to determine the shrinkage activity of the interconnect, electrode, seal and electrolyte tapes during both the debindering and the sintering step. To study the debindering step, the measurements are carried out in a TOMMI optical dilatometer (Fraunhofer Institut Silicatforschung ISC, Germany), in air atmosphere using green tapes rolled to a cylinder (5 mm diameter, 10 mm length). To study the sintering step, the measurements are carried out in a graphite heated thermos-optical measurement device (TOM_metal, Fraunhofer-Center for High Temperature Materials and Design, Germany), in reducing atmosphere using the debindered rolled tapes.

The microstructure of the as-prepared and tested monoliths is investigated on fractured and polished cross-sections by scanning electron microscopy (SEM) using a Hitachi TM3000 equipped with a Bruker energy dispersive X-ray spectroscopy (EDS) system, as well as with a Zeiss Merlin SEM equipped with a field emission gun.

Electrochemical cell testing

The single-cell monoliths are tested in a FuelCon Evaluator test rig for electrochemical performance. A metal test house was constructed to supply gasses to the cell and to allow for fast heating/cooling. The monolith is placed in the metal test house as shown in Fig. 4, using mica for sealing. Gas tightness is achieved by screwing the two parts of the cell house together. Probes for voltage/current are placed at equidistance from the sides of the cell. The fuel-inlet and -outlet are located on the long side of the monolith while air-inlet and -outlet are placed on the short side, as shown in Fig. 4b.

The monolith is heated at 10 °C/h to 650 °C feeding 5% H_2 balanced with N_2 (10 $_N$L/h) to the fuel electrode and air (10 $_N$L/h) to the oxygen electrode. At 650 °C, the 5% H_2/N_2 is replaced with pure H_2 (10 $_N$L/h).

For durability tests, cells A and B were tested under current (450 mA/cm^2 and 170 mA/cm^2, respectively), while cells C and D were kept at OCV. Cell A was tested at 800 °C feeding 60 $_N$L/h of air to the air electrode and 25 $_N$L/h of H_2 to the fuel electrode. Cells B, C and D were tested at 650 °C feeding 10 $_N$L/h of air to the air electrode and 10 $_N$L/h of H_2 to the fuel electrode.

Results and discussion

Processing optimization to produce crack-free monolith

Manufacturing monolithic SOFCs is complex and challenging as it requires co-sintering of ceramic and metal materials spread over several layers, of which some must be highly porous (e.g. electrodes about 50% porous) while others must be fully dense (e.g. electrolyte, sealing). To achieve this while avoiding cracks and delamination between the different layers, the sintering behaviour of each component of the cell has to be optimized, for example by tailoring the slurry composition and/or the particle sizes of the raw materials.

To aid with this optimization, dilatometry measurements are performed on tapes constituting individual components of the cell to study their shrinkage behaviour. As the interconnect constitutes the thickest layer of the monolith (see Fig. 1) it will direct the overall shrinkage during sintering. The cell components that do not follow the shrinkage behaviour of the interconnect will be put under either compressive stress or tensile stress, which may lead to cracking or delamination. To

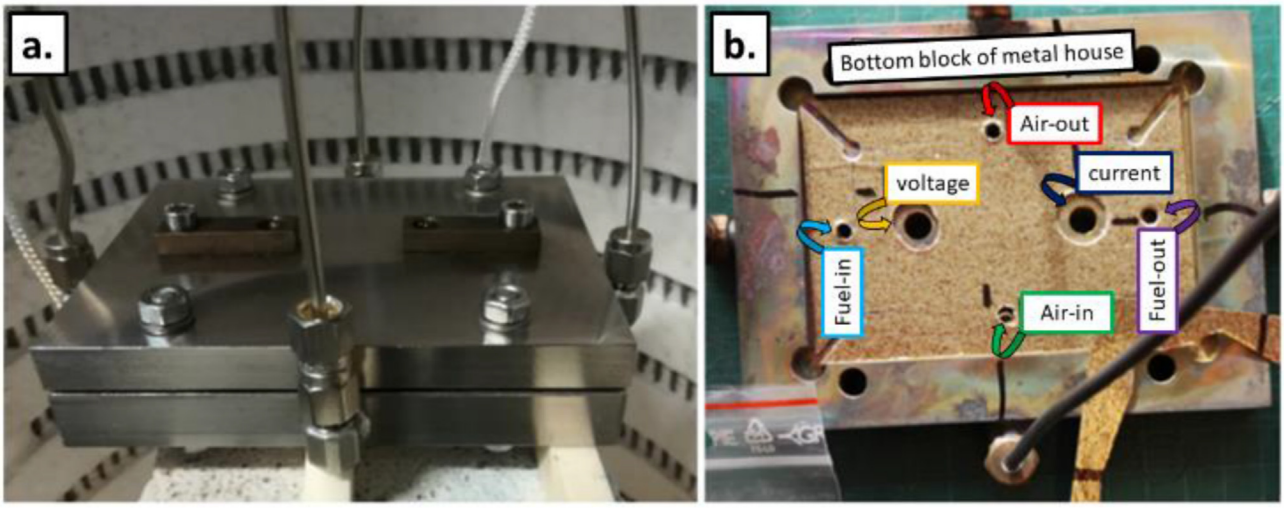

Fig. 4 – Pictures of the test house closed (a.) and opened (b.).

avoid this, the shrinkage mismatch between the interconnect and the other cell components should be minimized. The most critical cell component in this sense is the electrolyte, as in-sufficient gas-tightness of this layer (due to cracks or porosity) will lead to fuel cross-over and consequentially, significant performance loss.

Fig. 5 presents dilatometry measurements performed on rolled interconnect and electrolyte tapes during the debindering and sintering steps. The results show that from 25 °C to 1000 °C, the electrolyte shrinks about 1% less than the interconnect tape, which would result in slight compression of the electrolyte when the two layers are sintered together in a laminated structure. Above 1000 °C, the electrolyte shrinks more than the interconnect, which in a laminated structure translates to the electrolyte being put in tension. The greatest shrinkage mismatch between the two tapes is observed at 1250 °C and corresponds to 8% of the relative length. At 1290 °C, the shrinkage mismatch decreases and the electrolyte is put in compression again. Note that the electrolyte is less likely to fracture under compressive stress than tensile stress [25]. Overall, the shrinkage mismatch between electrolyte and interconnect is rather small and the electrolyte is mostly in compression during the firing process. These conditions facilitate the fabrication of crack-free monolithic SOFCs.

While matching the shrinkage behaviour of the cell components is essential to produce crack-free monolithic SOFCs, there are also other factors that can lead to cracking and/or poor adhesion of adjacent layers, for example thermal expansion mismatch, or defects introduced through the manufacturing.

After many rounds of process optimization, the following approaches and parameters were found essential to achieve crack-free monoliths: (i) co-casting of seals and electrodes, (ii) the composition of the seals, and (iii) the joining of the layers. Fig. 6 shows selected cross-sections of the monolith, which illustrate the structural evolvement through these optimizations. Firstly, co-casting adjacently and simultaneously seals and electrodes help to ensure a good adhesion of these components and to protect the electrolyte from cracking (Fig. 6b). Past experiments proved that when seals and electrodes are tape-casted separately and laminated adjacently, there is no adhesion (see Fig. 6a, blue rectangle), which weakens and fractures the electrolyte (see Fig. 6a, green rectangle). Secondly, the composition of the seals was changed from pure ceramic to a mixture of ceramic and metal (cermet). The use of purely ceramic seals generates cracks in the seal and the electrolyte (see Fig. 6c, red rectangle) and/or at the seal/electrolyte interface, probably due to the TEC mismatch between the purely metallic interconnects and the purely ceramic seals and electrolyte. Once 20 vol% of metal is added to the composition of the seals, no more cracks are observed (see Fig. 6d). Finally, the method used to join green tapes together and form the monolithic SOFCs was changed. Initially, a standard laminator consisting of heated rolls in a double roll set-up was used to laminate the green tapes together. Such a device allows for controlling the temperature of the rolls, but not the pressure applied to the tapes. Consequently, the electrodes and the electrolyte are significantly deformed during lamination as shown by the orange rectangle in Fig. 6e. These deformations occasionally fracture the electrodes and the electrolyte. Such defects are avoided by using an isostatic press to join the green tapes. Note that hypothetically any equipment controlling the pressure applied and the temperature could be used. The press is set to 85 °C and 30 MPa, and the lamination is performed for 10 min. This technique allows for keeping the electrodes and the electrolyte flat during the manufacturing process (see Fig. 6f).

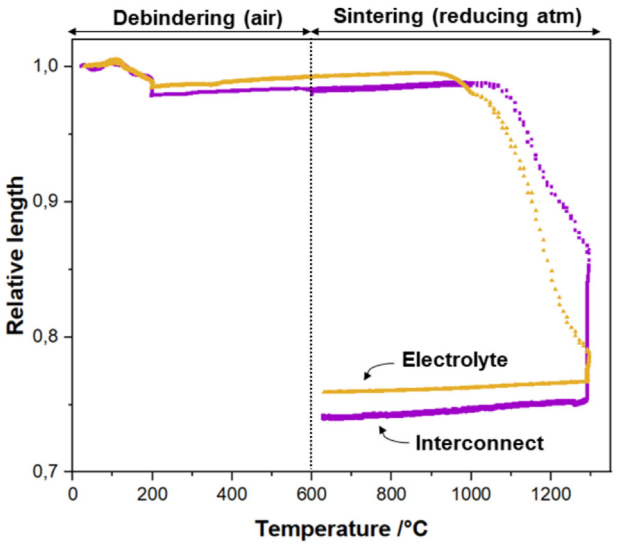

Fig. 5 – Dilatometry measurements performed on interconnect and electrolyte rolled tapes under air from 25 °C to 600 °C and under reducing atmosphere from 600 °C to 1290 °C.

Electrochemical performance

Initial electrochemical performances

Polarization curves (iV-curves) are recorded to determine the initial electrochemical performance of single-cell monoliths. Fig. 7 shows the polarization curves for selected cells at temperatures of 650 °C (cells B, C, D) and 750 °C (cell A). Dry hydrogen and either air or O_2 are supplied to the fuel and oxygen electrodes, respectively. Three cell characteristics can be extracted from the polarization curves, the OCV, the power density and the area specific resistance (ASR). The recorded OCV values are between 1100 and 1140 mV. The OCV value is a measure of the gas tightness of the cell/setup. For a well-established test setup and a standard anode supported SOFC an OCV of 1200 mV is achievable. This shows that the gas tightness of the innovative monolith/setup is similar to the benchmark value. In addition to gas leaks, an electronic leak across the electrolyte will cause a lower OCV. The monolith has a higher risk of such a short circuit as it mainly consists of metal. The short circuit is not a large issue and can be solved with minor efforts.

The apparent active cell area of the monolith cell is estimated to be 3 × 6 cm^2 based on the area covered by the gas channels (see Fig. 3). This active area of 18 cm^2 is used in the calculation of the current densities in the polarization curves (Fig. 7) and the corresponding ASR values reported in Table 1. However, non-ideal contacting in this new and innovative cell test set-up (compared to a traditional cell test set-up described

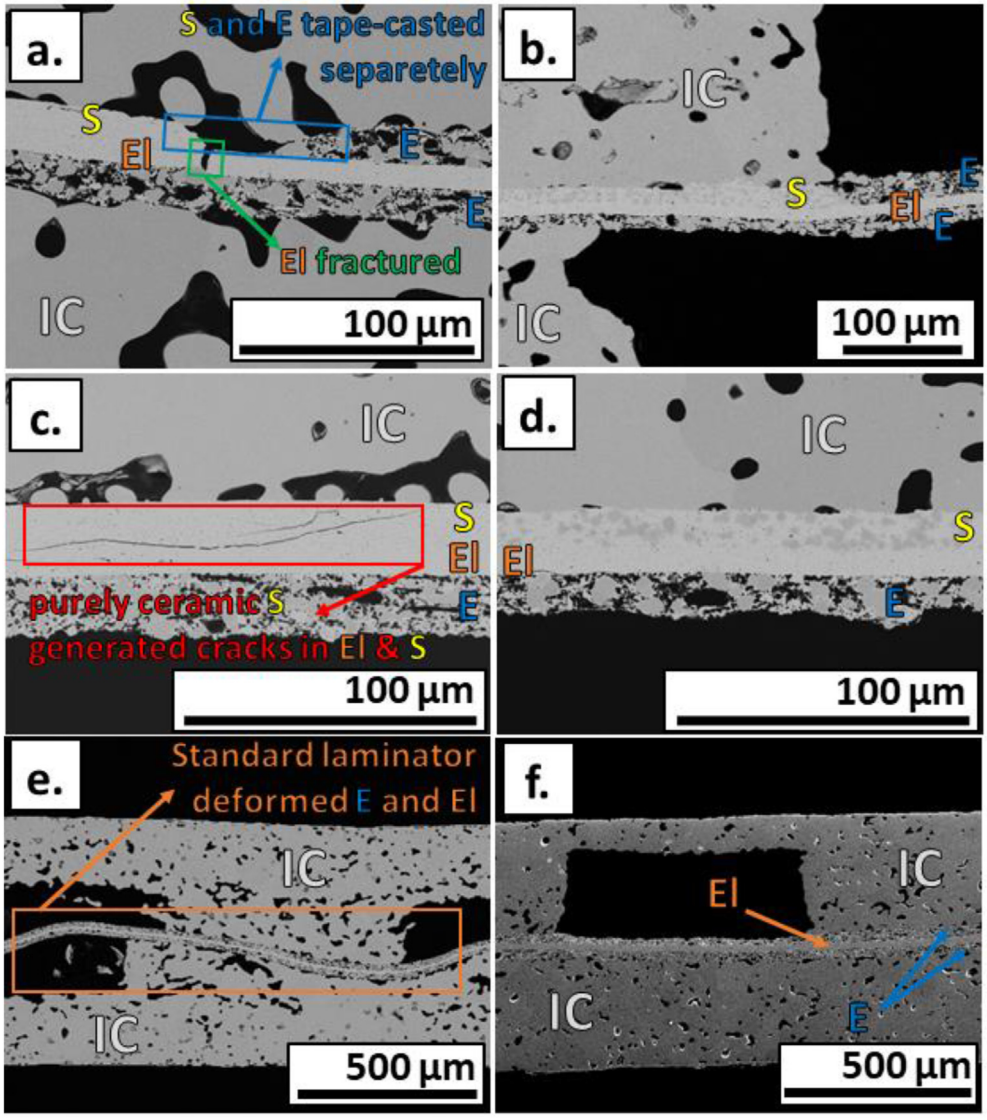

Fig. 6 – Processing optimization to fabricate crack-free monolithic SOFCs. a. Example of cell fabricated with seals and electrodes tape-casted separately and laminated adjacently, b. Example of cell produced with side-by-side tape-casting of seal/electrode, c. Example of cell containing pure ceramic seals, d. Example of cell containing cermet seals, e. Example of cell laminated via standard laminator (heated rolls) and f. Example of cell laminated via isostatic press. In this figure, S=Seal, IC=Interconnect, El = Electrolyte, and E = Electrode.

elsewhere for ceramic cells [26]) might result in an active cell area smaller than 18 cm^2 during testing. Such possible error on the assumed contact area implies that the "real" ASR values may be lower, but not higher, than the values given in Table 1. Note that the ASR values stated are not corrected for fuel utilization [27].

The ASR values from the different cells span from the lower performing cell D having an ASR of 6.9 Ω cm^2 (at 650 °C) to the highest performing cell (cell A) having an ASR of 0.7 Ω cm^2 (at 750 °C). Although cell A was tested at higher temperature, the improvement in performance is evident. The increased performance (lower ASR) from cell D to cell A illustrates the improved electrode microstructure and catalyst infiltration. In cell A, the porosity of the electrodes and the metallic layers surrounding the gas channels was increased to facilitate catalyst infiltration in the electrodes and therefore enhance the electro-catalytic activity. The development of cell D was focused on improving the mechanical properties of the cell (see sub-section 4.2.2. and Fig. 8) and the cell has non-optimal electrode structures and infiltration, which cause the higher ASR. The maximal power density was recorded on Cell A, it corresponds to 0.48 W cm^{-2} at 750 °C. This value can be compared to the power density of conventional metal supported SOFC recently developed by Hu et al. [28], reaching 0.26 W cm^{-2} at 750 °C.

The monolithic SOFC presented in this work is still in its initial development state and as expected, the ASR values of these cells are still significantly higher than for more conventional and matured metal supported cells reported lately. For example, Hagen et al. reported performances of

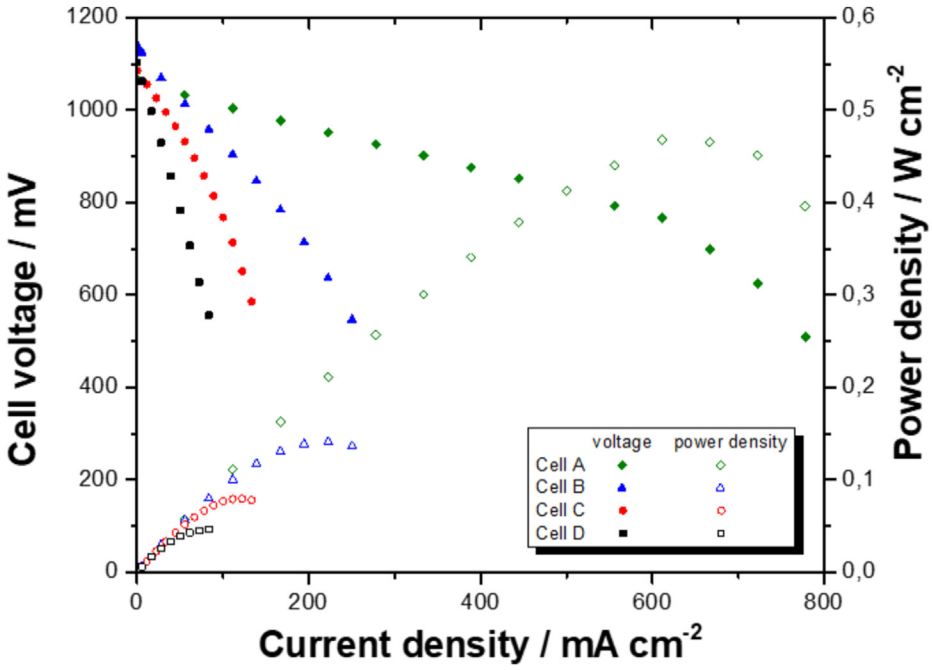

Fig. 7 – Polarization curves recorded at 650 °C (cells B, C and D) and 750 °C (cell A), dry hydrogen to the fuel electrode, and air (cells B, C and D) or oxygen (cell A) to the oxygen electrode. See Table 1 for further listing of specification of cells and results from the polarization curves.

Table 1 – Key numbers and characteristics from electrochemical tests of single-cell monoliths. OCV is given at 650 °C, dry H_2 and air. ASR value is calculated as the slope of the polarization curves from OCV to the maximum current density given in Fig. 7. Cell development during durability tests are depicted in Fig. 8.

Cell name	OCV before polarization curve (mV)	ASR (T) (Ωcm^2)	Durability test conditions	Durability test results	Key processing parameters
cell A	1100	0.7[a] (750 °C)	t = 3 h T = 800 °C; j = 450 mA/cm^2 Q_{H_2} = 25 $_N$L/h; Q_{air} = 60 $_N$L/h	$E_{t=0}$ = 649 mV $E_{t=3h}$ = 195 mV	- Seals and electrodes tape-casted separately - Purely ceramic seals - Standard laminator
cell B	1140	2.3 (650 °C)	t = 42 h T = 650 °C; j = 170 mA/cm^2 Q_{H_2} = 10 $_N$L/h; Q_{air} = 10 $_N$L/h	$E_{t=0}$ = 1139 mV $E_{t=42h}$ = 45 mV	- Side-by-side casting seal/electrode/seal - Purely ceramic seals - Standard laminator
cell C	1104	3.6 (650 °C)	t = 48 h T = 650 °C; j = 0 mA/cm^2 Q_{H_2} = 10 $_N$L/h; Q_{air} = 10 $_N$L/h	$E_{t=0}$ = 1084 mV $E_{t=48h}$ = 108 mV	- Side-by-side casting seal/electrode/seal - Purely ceramic seals - Standard laminator
cell D	1132	6.9 (650 °C)	t = 319 h T = 650 °C; j = 0 mA/cm^2 Q_{H_2} = 10 $_N$L/h; Q_{air} = 10 $_N$L/h	$E_{t=0}$ = 1110 mV $E_{t=319h}$ = 373 mV	- Side-by-side casting seal/electrode/seal - Cermet seals - Laminated via isostatic press

t = duration of the test, j = current density applied, T = temperature, Q_{H_2} = gas flow of H_2, Q_{air} = gas flow of air, E = cell voltage.
[a] ASR value calculated as the slope of the polarization curves from 0 to 600 mA cm^{-2}

conventional planar metal supported cells reaching 0.8 Ωcm^2 at 650 °C, using a hydrogen fuel containing 20% of steam thus not identical to the fuel in the study [29]. Further improvements of the monolith performance are to be expected if the electrodes microstructure and the infiltration procedure are improved and if more active electrocatalysts are used [30,31]. In general, the cells do not seem to suffer from fuel or oxygen starvation; only the polarization curve for cell A could be interpreted as starting to reach fuel and/or oxygen starvation and/or mass transport limitation at current densities above 0.6 A/cm^2; however no systematic investigation (flow variations) of possible fuel and or oxygen starvation was conducted.

Durability

Fig. 8 shows the durability test for the monolith cells in terms of cell voltage over time. Two of the single-cell monoliths were tested under current (cells A and B), while the other two were kept at OCV (cells C and D). Cell A fails in less than 5 h while cells B and C degrade rapidly within less than 50 h. These failures are mainly due to leaks originating from cracks in the electrolyte and corrosion on the metal containing layers.

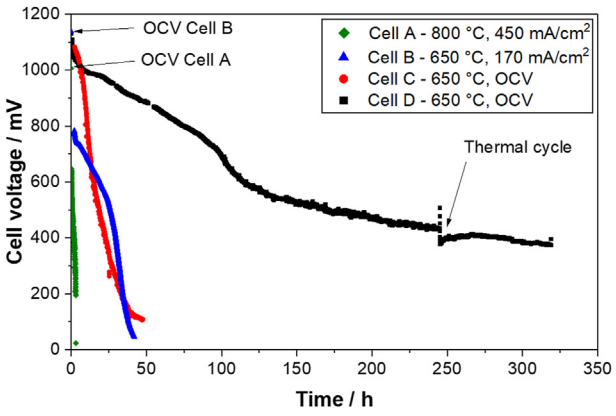

Fig. 8 – Cell voltage measured over time for cells A, B, C and D. All durability tests were performed supplying dry hydrogen and air to the fuel and oxygen electrodes, respectively. Key numbers from the durability tests are summarized in Table 1.

Despite this fast decrease of the cell voltage, it is clear that each improvement in the processing (cf. Table 1) significantly increased the durability from cell A to cells B & C and, finally cell D. Cell D, which incorporates all of the processing improvements (i.e. side-by-side tape casting, cermet sealing, and isostatic lamination) consequentially displays the longest lifetime. Furthermore, cell D did not take significant damage from being exposed to a thermal cycle down to room temperature.

The two cells were prepared in the same way and had a similar OCV before imposing a current on cell B (cf. Table 1). The similar cell voltage development for the two cells indicates that it is not the current load which caused the rapid degradation. Instead, the rapid degradation is caused by corrosion, as will be seen from the post-test analysis presented in Section 4.3.

Post-test analysis

Fig. 9 presents post-test SEM images and EDS analyses performed on cells D and E. Cell E is a "sister cell" of cell D that was prepared in the same way but not tested. Cell E thus serves as a reference for evaluating the impact of the electrochemical test on the microstructure and the chemical composition of the cell.

The analyses show that after the electrochemical test, the air side of cell D is heavily corroded (Fig. 9 b and 9 d). Corrosion occurred around the gas channels, at the electrode/interconnect interface and along the outer part of the interconnect. EDS point analyses (Supplementary Fig. 2) reveal that the corrosion product corresponds to iron oxide. The oxidation of iron is associated with a volume expansion, which will induce stresses in the monolith that may eventually lead to cracks in the brittle electrolyte (see Supplementary Fig. 3) and between the individual layers of the monolith. Cracks in the electrolyte allow hydrogen from the fuel side to enter the air side, resulting in direct combustion and formation of steam on the air side. It is well known that due to increased Cr vaporization, steam increases the corrosion rate of stainless steels and can lead to break-down of the slower-growing chromia scale that normally is formed on Fe22Cr in dry conditions [32,33]. Thus, once the electrolyte is cracked, corrosion of the cell will accelerate, causing a rapid degradation in cell voltage as seen

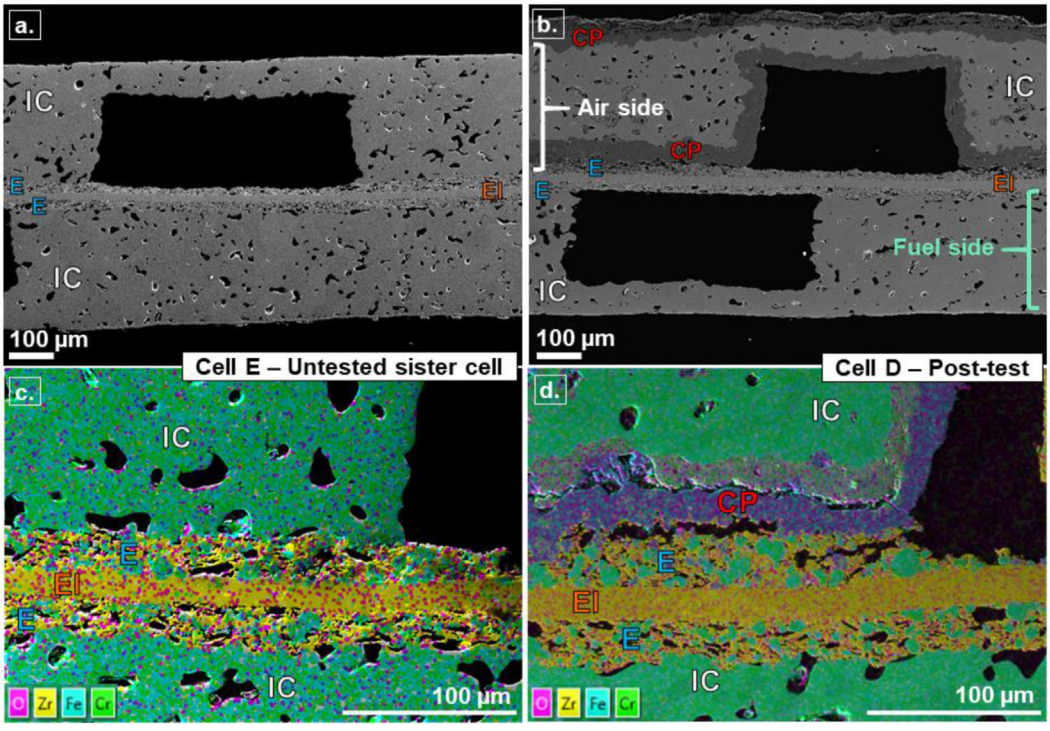

Fig. 9 – SEM images and EDS analyses of fractured and polished cross-sections of cell D (b. and d.) and cell E (a. and c.). In this figure, IC=Interconnect, El = Electrolyte, E = Electrode and CP = corrosion product.

in Fig. 8. We have previously shown that in dry air, corrosion proceeds much slower than observed here and that chromia is formed on the steel surface [10]. Thus, the anomalous oxidation observed after the electrochemical test can be attributed to leaks in the electrolyte, causing H_2 cross over to the cathode side and steam formation.

For cells A, B and C, cracks in the electrolyte were observed in references cells even before testing (see Fig. 6), which explains the rapid degradation of these cells. No cracks were found in the reference of cell D (cell E) but since only a small area of the cell is inspected in the cross-sectional SEM analysis it cannot be excluded that the cell contained a crack or pinhole somewhere in the electrolyte that could have acted as the starting point for the determinantal corrosion. Alternatively, the corrosion may have started in an area of the cell that is not well covered by the protecting CGO layer. Nevertheless, it is clear that the improvement in cell processing from cell A to cell D has a significant, positive impact on the cell durability.

Compared to conventional SOFCs, the monolith design presents the advantages of integrating gas flow channels and seals into a co-sintered block containing both a metallic substrate and ceramic cell interlayers resulting in high volume power density and improved in-plane thermal distribution. Moreover, only a single heat treatment is required for the manufacturing process, as opposed to two or three for conventional SOFCs. These advantages come with the cost of a very challenging manufacturing route which requires to co-sinter ceramic and metal materials spread over several layers and a wide range of porosity (from fully dense to highly porous). The study shows that preventing cracks in the electrolyte is crucial for the cell reliability and durability. This can be achieved by optimizing the sintering behaviour of each layer and improving their interfaces. Further work will be needed to (i) prevent corrosion of the interconnects and (ii) improve the electrochemical performance of the monolith. The corrosion of the interconnect could be solved by optimizing the infiltration of CGO to create a dense and continuous layer to protect against corrosion, or by developing new corrosion-resistant layers based on other materials. Currently, spinel-based coatings such as $(Mn,Co)_2O_4$ and $(Mn,Cu)_3O_4$ are considered the most promising for application on the SOFC air side, as they provide resistance against both oxidation and Cr volatilization [34–36]. Thus, these compositions can be considered in case the current solution of infiltrating a CGO layer proves insufficient for long-term corrosion resistance. The spinel-based coatings can also be realised by infiltration in porous metals, as demonstrated in Ref. [37].The electrochemical performance of the monolith could be boosted by maximizing the triple phase boundary junctions in the electrodes and infiltrating highly electro-active catalysts.

Conclusion

In this work, a novel monolithic metal supported SOFC is designed, manufactured, and tested. The monoliths are fabricated using cost competitive and scalable manufacturing methods such as tape-casting, lamination, and co-sintering. The initial OCV values recorded in air and H_2 (1100–1140 mV) indicate a tolerable gas tightness of the manufactured single-cell monoliths. The best performing cell displays an ASR of 0.7 Ωcm^2 at 750 °C in H_2, although limited efforts were made to optimize the cell performance. The stability of the single-cell monolith was improved by step-wise optimizations of the processing, including: side-by-side co-casting of seals and electrodes, adjustment of the composition of the seals, and amelioration in the lamination of the individual layers. However, although significant improvements were achieved, the lifetime is limited to ca. 300 h because of corrosion. In future works, the lifetime of the monoliths may be further improved by the development of corrosion-resistant layers. Also, the development of optimized electrode microstructure would boost the electro-catalytic activity of the cells.

Author contributions

S.P., B.T., K.B., T.L.S., and A.Hau. designed the experiments leading to the final monolith design. S.P. and K.B. manufactured the tested single-cell monoliths. S.P., K.B., and A.H.P. carried out preliminary experiments on manufacturing. T.L.S., S.P. and B.T. contributed to the fuel cell functionalization. B.T. contributed to the corrosion study. S.P. and B.T. performed the microscopy analyses. A.Hau., J.V.T.H. and H.H. conducted the electrochemical tests. A. Hag. supervised the research. S.P. wrote the initial manuscript. All the authors revised the manuscript.

Declaration of competing interest

The authors declare that they have no known competing financial interests or personal relationships that could have appeared to influence the work reported in this paper.

Acknowledgments

The authors gratefully acknowledge the financial support from Plastic Omnium. The authors are also grateful towards Henrik Paulsen for assisting in the preparation of samples for SEM/EDS analyses and Søren Christensen for assisting in the preparation of slurries for tape-casting.

Appendix A. Supplementary data

Supplementary data to this article can be found online at https://doi.org/10.1016/j.ijhydene.2022.12.139.

REFERENCES

[1] Minh NQ. Ceramic fuel cells. J Am Ceram Soc 1993;76:563–88.
[2] Singhal SC. Solid oxide fuel cells for stationary, mobile, and military applications. Solid State Ionics 2002;152–153:405–10. https://doi.org/10.1016/S0167-2738(02)00349-1.

[3] Föger K, Love JG. Fifteen years of SOFC development in Australia. Solid State Ionics 2004;174:119–26. https://doi.org/10.1016/j.ssi.2004.06.018.
[4] Lim TH, Park JL, Lee SB, Park SJ, Song RH, Shin DR. Fabrication and operation of a 1 kW class anode-supported flat tubular SOFC stack. Int J Hydrogen Energy 2010;35:9687–92. https://doi.org/10.1016/j.ijhydene.2010.06.052.
[5] Blum L, Meulenberg WA, Nabielek H, Steinberger-Wilckens R. Worldwide SOFC technology overview and benchmark. Int J Appl Ceram Technol 2005;2:482–92. https://doi.org/10.1111/j.1744-7402.2005.02049.x.
[6] Blennow P, Hjelm J, Klemensø T, Persson Å, Brodersen K, Srivastava A, Frandsen H, Lundberg M, Ramousse S, Mogensen M. Development of planar metal supported SOFC with novel cermet anode. ECS Trans 2009;25:701–10. https://doi.org/10.1149/1.3205585.
[7] Sammes NM, Du Y. Fabrication and characterization of tubular solid oxide fuel cells. Int J Appl Ceram Technol 2007;4:89–102. https://doi.org/10.1111/j.1744-7402.2007.02127.x.
[8] Huang K, Singhal SC. Cathode-supported tubular solid oxide fuel cell technology: a critical review. J Power Sources 2013;237:84–97. https://doi.org/10.1016/j.jpowsour.2013.03.001.
[9] Singhal SC. Advances in solid oxide fuel cell technology. Solid State Ionics 2000;135:305–13. https://doi.org/10.1016/S0167-2738(00)00452-5.
[10] Pirou S, Talic B, Brodersen K, Hauch A, Frandsen HL, Skafte TL, Persson ÅH, Høgh JVT, Henriksen H, Navasa M, Miao X-Y, Georgolamprou X, Foghmoes SPV, Hendriksen PV, Nielsen ER, Nielsen J, Wulff AC, Jensen SH, Zielke P, Hagen A. Production of a monolithic fuel cell stack with high power density. Nat Commun 2022;13:1–8. https://doi.org/10.1038/s41467-022-28970-w.
[11] Larsen PH, Smith A, Mogensen M, Linderoth S, Hendriksen PV. Reversible solid oxide fuel cell stack and method for preparing same. EP1760817B1; 2005.
[12] Carter JD, Myers D, Kumar R. Bipolar Plate supported solid oxide fuel cell with a self-sealed anode compartment. In: Fuel cell semin.; 2005.
[13] Park S, Sammes NM, Song K-H, Kim T, Chung J-S. Monolithic flat tubular types of solid oxide fuel cells with integrated electrode and gas channels. Int J Hydrogen Energy 2017;42:1154–60.
[14] Heck RM, Gulati S, Farrauto RJ. The application of monoliths for gas phase catalytic reactions. Chem Eng J 2001;82:149–56. https://doi.org/10.1016/S1385-8947(00)00365-X.
[15] Omar S, Bin Najib W, Chen W, Bonanos N. Electrical conductivity of 10 mol% Sc2O3-1 mol% M2O3- ZrO2 ceramics. J Am Ceram Soc 2012;95:1965–72. https://doi.org/10.1111/j.1551-2916.2012.05126.x.
[16] Winkler W. Benefits and risks of mobile SOFC applications. Eur. Fuel Cell News. 1999;6:8–11.
[17] Peksen M, Al-Masri A, Blum L, Stolten D. 3D transient thermomechanical behaviour of a full scale SOFC short stack. Int J Hydrogen Energy 2013;38:4099–107. https://doi.org/10.1016/j.ijhydene.2013.01.072.
[18] Holgate TC, Han L, Wu N, Bøjesen ED, Christensen M, Iversen BB, Van Nong N, Pryds N. Characterization of the interface between an Fe-Cr alloy and the p-type thermoelectric oxide Ca3Co4O9. J Alloys Compd 2014;582:827–33. https://doi.org/10.1016/j.jallcom.2013.08.096.
[19] Wang ZZ, Bai Y, Fan W, Gao Y, Liu Q, Wang RJ, Tao WZ, Ma F. Effect of Sc substitution on thermophysical properties of tetragonal ScYSZ: molecular dynamics simulation. Comput Mater Sci 2020;174. https://doi.org/10.1016/j.commatsci.2019.109478.
[20] Mistler RE, Twiname ER. Tape Casting: theory and practice. Westerville, Ohio: The American Ceramic Society; 2000.
[21] Knibbe R, Wang HJ, Blennow P, Thydén K, Persson ÅH, Mikkelsen L, Klemensø T. Oxidation in ceria infiltrated metal supported SOFCs-A TEM investigation. J Power Sources 2013;228:75–82. https://doi.org/10.1016/j.jpowsour.2012.11.051.
[22] Klemensø T, Chatzichristodoulou C, Nielsen J, Bozza F, Thydén K, Kiebach R, Ramousse S. Characterization of impregnated GDC nano structures and their functionality in LSM based cathodes. Solid State Ionics 2012;224:21–31. https://doi.org/10.1016/j.ssi.2012.07.011.
[23] Ovtar S, Chen M, Samson AJ, Kiebach R. In-situ formed Ce0.8Gd0.2O1.9 barrier layers on yttria stabilized zirconia backbones by infiltration - a promising path to high performing oxygen electrodes of solid oxide cells. Solid State Ionics 2017;304:51–9. https://doi.org/10.1016/j.ssi.2017.03.019.
[24] Talic B, Molin S, Hendriksen PV, Lein HL. Effect of pre-oxidation on the oxidation resistance of Crofer 22 APU. Corrosion Sci 2018;138:189–99. https://doi.org/10.1016/j.corsci.2018.04.016.
[25] Bermejo R, Baudín C, Moreno R, Llanes L, Sánchez-Herencia AJ. Processing optimisation and fracture behaviour of layered ceramic composites with highly compressive layers. Compos Sci Technol 2007;67:1930–8. https://doi.org/10.1016/j.compscitech.2006.10.010.
[26] Ebbesen SD, Graves C, Hauch A, Jensen SH, Mogensen M. Poisoning of solid oxide electrolysis cells by impurities. J Electrochem Soc 2010;157:B1419. https://doi.org/10.1149/1.3464804.
[27] Mogensen M, Hendriksen PV. Chapter 10: testing of electrodes, cells and short stacks. Elsevier Ltd; 2003. https://doi.org/10.1016/B978-185617387-2/50027-1.
[28] Hu B, Lau G, Song D, Fukuyama Y, Tucker MC. Optimization of metal-supported solid oxide fuel cells with a focus on mass transport. J Power Sources 2023;555:232402. https://doi.org/10.1016/j.jpowsour.2022.232402.
[29] Hagen A, Sun X, Sudireddy BR, Persson ÅH. Metal supported SOFCs for mobile applications using hydrocarbon fuels. J Electrochem Soc 2020;167:104510. https://doi.org/10.1149/1945-7111/ab9b9d.
[30] Dogdibegovic E, Wang R, Lau GY, Karimaghaloo A, Lee MH, Tucker MC. Progress in durability of metal-supported solid oxide fuel cells with infiltrated electrodes. J Power Sources 2019;437:226935. https://doi.org/10.1016/j.jpowsour.2019.226935.
[31] Dogdibegovic E, Wang R, Lau GY, Tucker MC. High performance metal-supported solid oxide fuel cells with infiltrated electrodes. J Power Sources 2019;410–411:91–8. https://doi.org/10.1016/j.jpowsour.2018.11.004.
[32] Sachitanand R, Svensson JE, Froitzheim J. The influence of Cr evaporation on long term Cr depletion rates in ferritic stainless steels. Oxid Metals 2015;84:241–57. https://doi.org/10.1007/s11085-015-9552-5.
[33] Saunders SRJ, Monteiro M, Rizzo F. The oxidation behaviour of metals and alloys at high temperatures in atmospheres containing water vapour: a review. Prog Mater Sci 2008;53:775–837. https://doi.org/10.1016/j.pmatsci.2007.11.001.
[34] Talic B, Falk-Windisch H, Venkatachalam V, Hendriksen PV, Wiik K, Lein HL. Effect of coating density on oxidation resistance and Cr vaporization from solid oxide fuel cell interconnects. J Power Sources 2017;354:57–67. https://doi.org/10.1016/j.jpowsour.2017.04.023.

[35] Mikkola J, Couturier K, Talic B, Frangini S, Giacometti N, Pelissier N, Sudireddy BR, Thomann O. Protective coatings for ferritic stainless steel interconnect materials in high temperature solid oxide electrolyser atmospheres. Energies 2022;15. https://doi.org/10.3390/en15031168.

[36] Bianco M, Tallgren J, Hong JE, Yang S, Himanen O, Mikkola J, Van herle J, Steinberger-Wilckens R. Ex-situ experimental benchmarking of solid oxide fuel cell metal interconnects. J Power Sources 2019;437:226900. https://doi.org/10.1016/j.jpowsour.2019.226900.

[37] Stefan E, Neagu D, Blennow Tullmar P, Persson ÅH, Sudireddy BR, Miller D, Chen M, Irvine J. Spinel-based coatings for metal supported solid oxide fuel cells. Mater Res Bull 2017;89:232–44. https://doi.org/10.1016/j.materresbull.2017.02.003.